NEXUS OF FROG VENTRICLE

ROBERT W. KENSLER, PETER BRINK, and MAYNARD M. DEWEY

From the Department of Anatomical Sciences, Health Science Center, State University of New York, Stony Brook, New York 11794

ABSTRACT

Here we demonstrate in *Rana pipiens* ventricle a nexus with very unusual morphology. This tissue has been reported previously to lack nexuses. The nexus appears in thin sections of ventricle, fixed in aldehyde and OsO_4 or permanganate, as a series of punctate membrane appositions regularly alternating with regions of membrane separation. The junctional width at membrane appositions, as determined by microdensitometry and optical measurements, is 15–17 nm, and the width of the electron-translucent region between the junctional membranes is 1.8 nm. These values correspond closely to similar measurements of the more typical nexuses in frog liver. Along the nexus the mean distance between punctate appositions is 74.5 nm.

Freeze-cleave replicas of the nexuses between myocardial cells show particles 10.4 nm in diameter arranged in arrays of up to nine linked circles or partial circles on the PF-face and similar arrays of pits of shallow grooves on the EF-face. The mean diameter of the circles on both membrane fracture faces is 76.7 nm. A comparison of the thin-sectioned and freeze-cleaved nexuses demonstrates an excellent correspondence between the spacing of membrane appositions along the junction and the diameters of the freeze-cleaved circles of particles and pits or grooves.

Compelling evidence exists for the propagation of action potentials along vertebrate cardiac cells by the electrotonic spread of current across low resistance junctions. Such electrotonic spread of current has been demonstrated in Purkinje fibers (45), rat atrium (47), calf and sheep ventricle (46), and frog atrium (2, 4, 43). Correlated electrophysiological and morphological studies in guinea pig papillary muscle and frog atrial muscle (4) and rat ventricular muscle (16) have demonstrated that the nexus[1] is the intercellular junction associated with the electrotonic coupling of these cardiac cells. Additional support for the involvement of the nexus in the electrotonic coupling of cells comes from similar experiments with smooth muscle (3), the crayfish septate giant axon (28, 29), tissue culture cells (17, 19), and the fish nervous system (5–8).

In the ventricle of *Rana pipiens,* nexuses have been reported to be absent or not unequivocally demonstrated (38–40, 42). The failure to demonstrate nexuses in frog ventricle is difficult to reconcile with the evidence for electrotonic coupling of

[1] We have chosen to continue to use the term nexus for the junction described here. This usage is only a slight modification of Sherrington's (Sherrington, C. S. 1906. The Integrative Action of the Nervous System. Yale University Press; New Haven, Conn. 15–17) use of the term nexus to designate functional connections between cells. We believe that the term gap junction draws attention away from the physiologically important aspects of this junction.

frog cardiac cells (2, 4, 43, 44) and with the widespread occurrence of nexuses in the hearts of animals belonging to most of the major vertebrate classes (4, 20, 25, 26).

Previously, many nonmammals such as the axolotl, goldfish, turtle and chicken were also thought to lack nexuses. These species have now been shown to possess nexuses much shorter in length and much sparser in distribution than mammalian cardiac nexuses (25). The possibility existed that the frog ventricle might also possess unusual nexuses not clearly identified previously either because the junctions were labile under tissue preparative conditions (14), or because the junctions have an unusual morphology.

For this reason, we have investigated the intercellular junctions in the ventricle of *Rana pipiens*. We report the demonstration and characterization of a nexus with very unusual morphology and present a model for the structure of this nexus.

MATERIALS AND METHODS

Rana pipiens obtained from West Jersey Biological Farm, Wenonah, New Jersey were maintained at 20°C in running tap water, with forced feeding twice weekly. Males and females (sex determined by macroscopic observation) were studied during all seasons. Osmolarities were determined with an Advanced DigiMatic osmometer (Advanced Instruments, Inc., Needham Heights, Mass.).

Dissection and Fixation

The heart was excised from pithed frogs and placed in Ringer's solution containing 6.5 g of NaCl, 0.14 g of KCl, 0.12 g of $CaCl_2$, 0.2 g of $NaHCO_3$, 2.0 g of glucose, and 0.01 g of NaH_2PO_4 per liter. The ventral ventricular wall was incised from the atria to the ventricular tip, and the heart pinned open on a sheet of plastic. Some hearts were fixed immediately, some were allowed to recover from the trauma of dissection for 1 h before fixation, and others were further dissected before fixation. In the latter procedure, small 200–500-μm diameter bundles were dissected free, leaving only one end attached to the remainder of the heart including the sinus venosus; all continued to beat or were rejected. The dissected heart with isolated bundles was incubated for 1 h in Ringer's solution and then fixed. Hearts were also fixed by injecting the fixative into the *in situ* ventricle of a pithed frog. These hearts were excised and immersed in fresh fixative and dissected into cubes 1 mm on a side.

Frog liver was fixed by perfusing aldehyde fixative through the aorta. Successful fixation of the liver was judged by a blanching and hardening of the liver. The fixed liver was excised, placed in fresh fixative, and dissected into cubes 1 mm on a side.

A variety of glutaraldehyde fixatives were tested. A modified Karnovsky's fixative (21) containing 1.5% glutaraldehyde and 1.5% paraformaldehyde in 170 mosM sodium cacodylate buffer, pH 7.4 (total fixative osmolarity of 831 mosM) yielded the optimum fixation and unless otherwise specified was the aldehyde fixative employed. Tissues were fixed in the aldehyde fixative for 4–5 h, rinsed overnight in 170 mosM cacodylate buffer containing 20 mg/ml sucrose (total buffer rinse osmolarity of 230 mosM), and postfixed for 3 h in 2% OsO_4 in 230 mosM cacodylate buffer (pH 7.4). All fixative and buffer solutions were maintained at ±4°C, and most of them contained 0.5 mg/ml of anhydrous $CaCl_2$. Postfixed tissues were rinsed with 230 mosM sodium maleate buffer (pH 5.0) and *en bloc* stained with 2% uranyl acetate in the same buffer, either at room temperature or at 60°C.

The permanganate fixative contained 50 ml of 1.66% sodium permanganate solution, 20 ml of a stock veronal acetate solution (2.84 g of sodium barbital and 1.15 g of anhydrous sodium acetate in 100 ml water), 0.28 g of NaCl, 0.04 g of KCl, 0.02 g of $CaCl_2$, and 0.02 g of $MgCl_2$, all diluted to a total vol of 133 ml. The pH was set to pH 7.5 with HCl. Isolated bundles were fixed for 2 h at ±4°C and rinsed repeatedly in Ringer's solution before dehydration.

Ruthenium red (practical grade, 20% dye content, Sigma Chemical Co., St. Louis, Mo.) was employed as a tracer of the extracellular space (23, 24). Isolated bundles were fixed for 4–5 h in the aldehyde fixative, rinsed overnight at ±4°C in 230 mosM cacodylate buffer (pH 7.4) containing 10 mg/ml ruthenium red and postfixed for 3 h at room temperature in 2% OsO_4 in the same buffer containing 10 mg/ml ruthenium red. The tissue was *en bloc* stained as described above. All tissues prepared for thin sectioning were dehydrated in acetone (4°C) followed by propylene oxide and were embedded in Epon-Araldite plastic. Silver sections were cut on an LKB Ultrotome III (LKB Instruments, Inc., Rockville, Md.), collected on uncoated grids, and stained (with the exception of the ruthenium red-stained tissue) for 10 min with 2% uranyl acetate in 50% methanol and for 3 min in Reynolds's lead citrate (36).

Freeze-Fracture Studies

Frog hearts were excised from pithed frogs, pinned open, and incubated for 1 h in Ringer's solution. Some hearts were fixed for 1–2 h in the aldehyde fixative and bathed in 30% glycerol for 3–4 h at room temperature. Other hearts were immersed (without prior fixation) in 10% and 20% glycerol (1 h in each solution) and subsequently in 30% glycerol for 1–2 h at room temperature. Frog liver fixed by perfusion was soaked in 30% glycerol for 3–4 h at room temperature. All glycerol solutions contained 230 mosM cacodylate buffer. Small pieces of the glycerinated tissue rapidly frozen in liquid Freon 22 and liquid nitrogen were fractured and replicated at

−115°C (pressure, 5×10^{-6} Torr) on a Balzer's BAF 300 freeze-etch device equipped with a platinum-carbon electron beam gun and quartz thin-film monitor (Balzer's High Vacuum Corp., Santa Ana, Calif.). Platinum-carbon shadowing (2-nm thick film, 45° shadow angle) of the cleaved tissue was performed within 2 s of the last knife cut and was immediately followed by the deposition of a 20-nm thick carbon coat on the replica. The replicas were cleaned with Chlorox bleach, repeatedly rinsed with distilled water, and picked up on Formvar-coated 200-mesh grids. The micrographs are printed as positive images and the shadowing direction is indicated by an arrow in the lower right corner.

The freeze-cleave nomenclature proposed by Branton et al. (9) is employed to designate membrane fracture faces.

Electron Microscopy

All thin sections and freeze-cleave replicas were examined on a Hitachi HU-12 electron microscope at 75 kV. The electron optical magnification was calibrated with a 54,864 lines/inch replica of a diffraction grating (Ladd Research Industries, Inc., Burlington, Vt.). Photographs were taken on Kodak Contrast Lantern Slide Plates (Eastman Kodak Co., Rochester, N. Y.).

Measurements and Statistics

All electron micrographs utilized for both the microdensitometric measurements and the optical measurements were photographed at a magnification of 90,000.

MICRODENSITOMETRIC MEASUREMENTS: The structure of the nexus at the regions of closest membrane contact was reconstructed from microdensitometric tracings recorded with a Joyce, Loebl Mark IIIc microdensitometer (Joyce, Loebl and Co., Ltd., Gateshead-on-Tyne, England) at a total magnification of 4.5 million (scale: 1 mm on tracing = 0.2 nm in specimen). Microdensitometric reconstructions of frog liver nexuses were prepared for comparison. These junctional reconstructions were based on the principle that the width on a plate of a structure producing a microdensitometric peak is proportional to the width of the peak at its half-peak height, where the half-peak height is at the midpoint of a line constructed from the peak's apex perpendicular to the peak's base.

OPTICAL MEASUREMENTS: Electron micrograph plates were projected onto a screen with a Durst F-30 enlarger (Durst AG, Bolzano, Italy), and the measurements were made either directly from the projected image or from tracings of the image. The optical enlargement was calculated from the image size of a projected micrometer scale graduated in 0.1-mm units.

The total widths of the myocardial and liver nexuses were measured at a total magnification of 2,060,000 (scale: 1 mm on projected image = 0.48 nm). The intervals between the punctate appositions along the length of the myocardial nexuses and the distance of the cytoplasmic densities from the central plane of the nexus were mesured at a total magnification of 817,000 (scale 1 mm on projected image = 1.2 nm). The diameters of freeze-fractured particles in heart and liver nexuses were measured perpendicular to the direction of shadowing at a total magnification of 2,140,000 (scale: 1 mm on projected image = 0.47 nm). The diameters of the freeze-fractured rings of nexal particles and pits were determined from tracings of the junctions drawn from projections at a total magnification of 2,140,000 (scale: 1 mm on projected image = 0.47 nm). Circles which best fit the midpoints of each group of circularly arrayed particles or pits were constructed on the tracings, and their diameters measured. The mean and standard deviation of each set of values was determined with a Hewlett-Packard model 9830A computer (Hewlett-Packard Co., Palo Alto, Calif.).

RESULTS

Thin Sections: Aldehyde, OsO_4 and Permanganate Fixation

Only two types of intercellular junctions were observed in thin sections of frog ventricle fixed either in aldehyde and OsO_4 or in sodium permanganate. The first type, the fascia adherens, has previously been described in the frog heart (1, 4, 38, 42). The second type of intercellular junction, the nexus, was often found near the fascia adherens. This unusual nexus appears at low magnification as a specialized region of plasma membrane apposition similar to nexuses of other tissues but lacking the precise parallel arrangement of the juxtaposed plasma membranes (13, 14, 26). An unusual cytoplasmic density lies along each junctional membrane.

At higher magnification, the myocardial nexus frequently appears as two to seven punctate regions of membrane apposition regularly alternating with regions in which the junctional membranes diverge 5–15 nm apart (Figs. 1*b*, *d*, *f*, 2*a*, *c*, and *d*). At the points of membrane apposition, the aldehyde- and OsO_4-fixed nexus usually appears septalaminar with a 2.0-nm electron-translucent region between the junctional membranes (Fig. 1*b*, *d*, and *f*), and the permanganate-fixed nexus appears pentalaminar (Fig. 2*a*, *c*, and *d*). The mean periodic distance between the regions of membrane apposition along the length of the nexus is 74.5 nm (Fig. 3*b*). Figures 1*b*, *d*, and *f* illustrate the types of junctional regions measured. The junction may also appear as a short septalaminar nexus in aldehyde- and OsO_4-fixed ventricle (Fig. 4*a*) and as a short pentalaminar nexus in

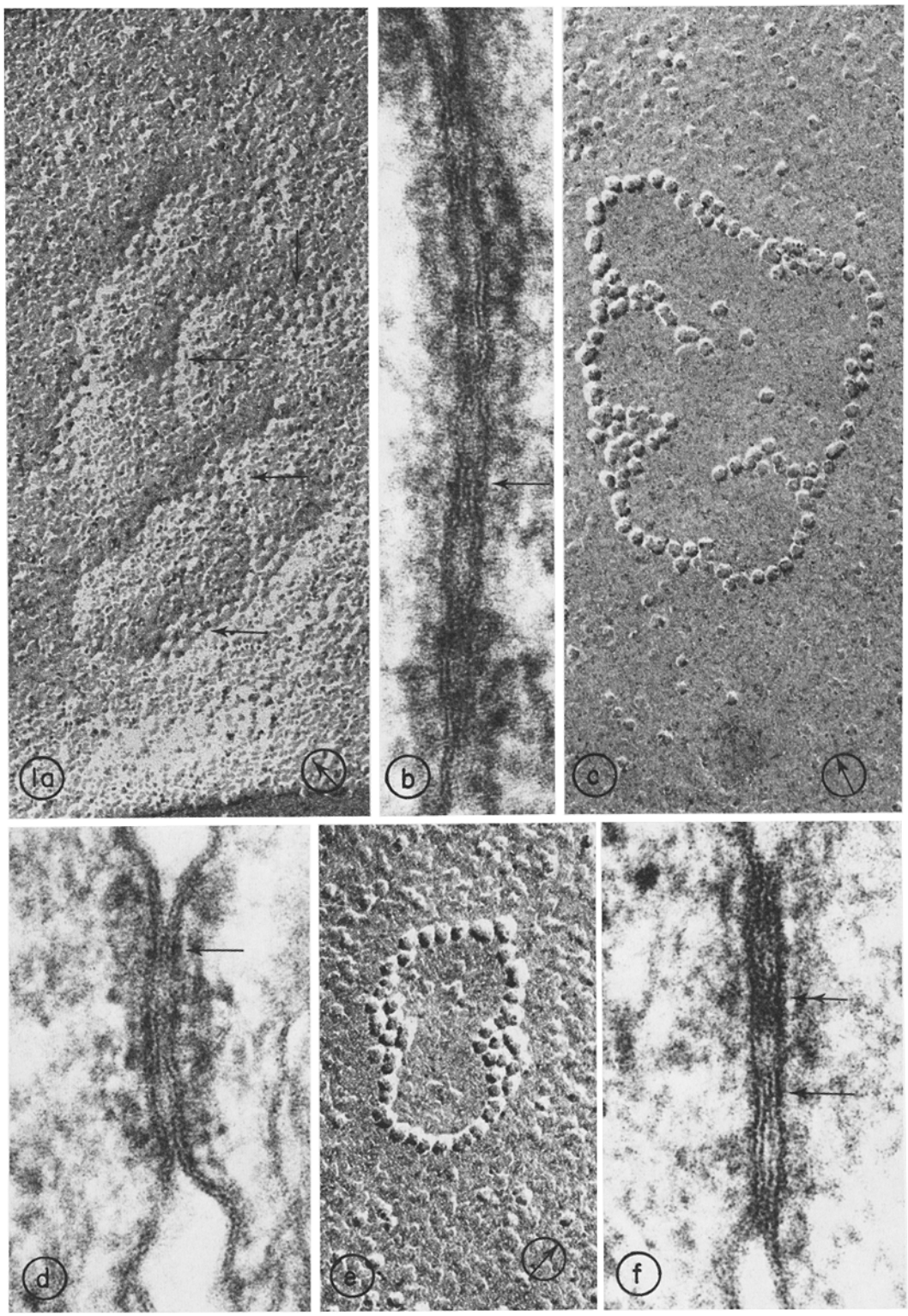

FIGURE 1 Comparison of the appearance of the aldehyde- and OsO_4-fixed myocardial nexuses in thin sections and in freeze-cleave replicas. All micrographs at × 240,000. (*a*) Freeze-cleave showing arrays of shallow pits and grooves of the EF face arranged in circles. The arrows point to small clusters of pits adjacent to the circles. The second arrow from the top points to a region in which one of the shallow grooves appears to consist of a line of pits. (*b*, *d*, and *f*) Thin-section images showing regions of membrane apposition alternating with regions of wider membrane separation. Arrows point to clear septalaminar membrane appositions. Note the appearance of the diffuse cytoplasmic densities along the junction. (*c* and *e*) Freeze-cleavage showing arrays of 10.4-nm particles on the PF face arranged in partial circles and adjacent clusters.

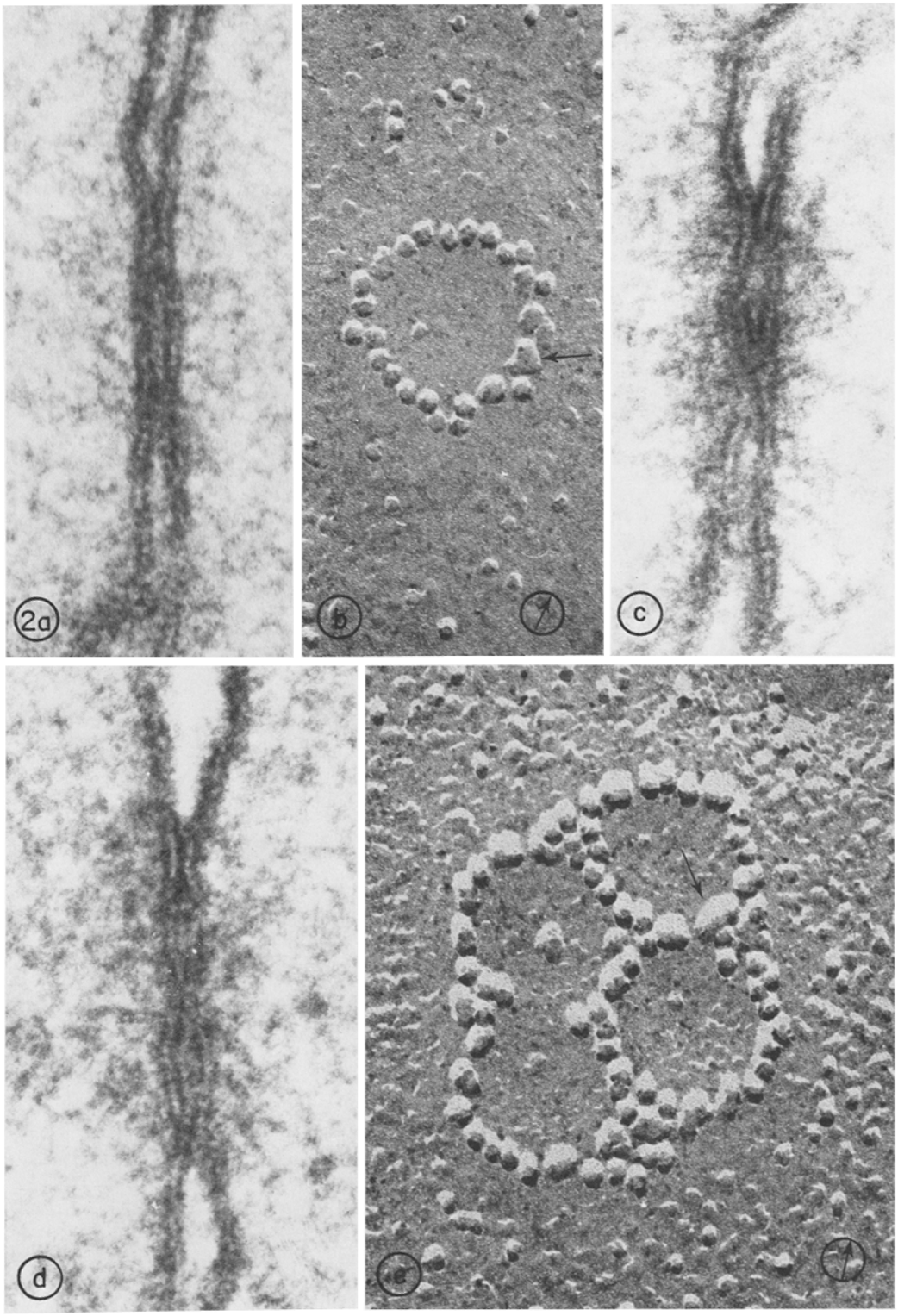

FIGURE 2 Comparison of the appearance of the permanganate-fixed myocardial nexuses in thin section and freeze-fractured images to illustrate the correspondence between the diameters of the freeze-fractured rings of particles and the distance between membrane apposition points along the junction. All micrographs at × 340,000. (*a*, *c*, and d) Thin-section images of a permanganate-fixed nexus illustrating membrane appositions alternating with regions of wider membrane separation. (*b* and *e*) Freeze-cleavage showing arrays of nexal particles arranged in circles on PF face. Arrows point to larger, irregularly shaped particles.

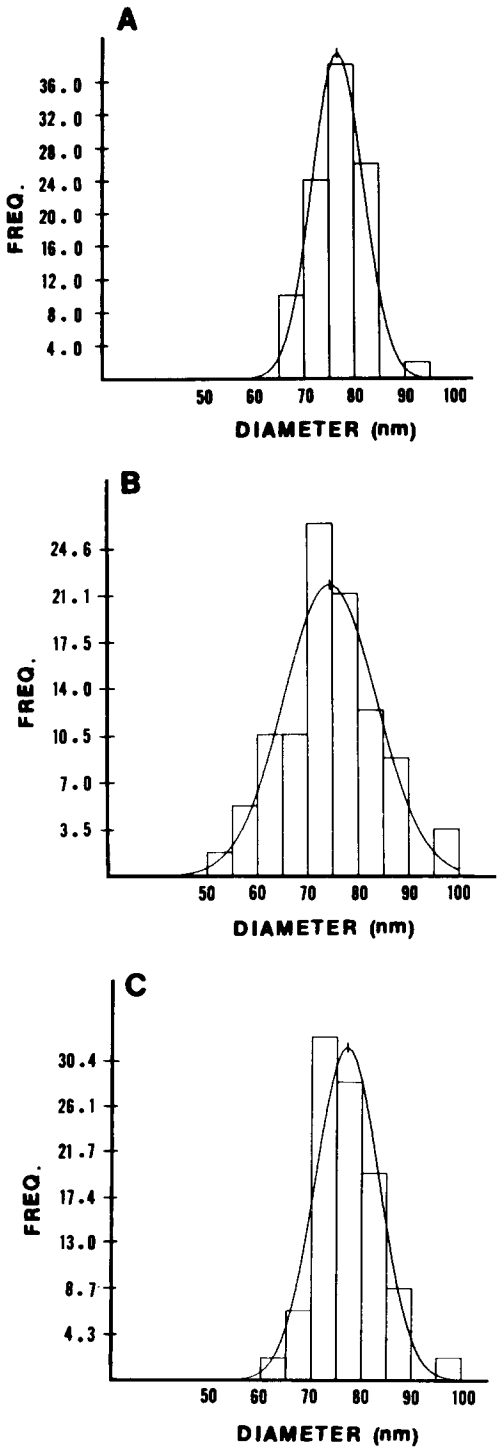

FIGURE 3 Histograms of the distributions of the diameters of rings of nexal particles on the PF-face (A) and the pits or grooves on the EF face (C), and the intervals between membrane appositions along the length of the thin-sectioned nexus (B). The mean diameter of the rings of particles was 76.7 SD 9.1 (n = 57), of the rings on the EF face 77.0 S.D. 6.3 nm (n = 46), and the mean distance between membrane appositions was 74.5 SD 9.1 nm (n = 57).

permanganate-fixed ventricle (Fig. 4*c*). The cytoplasmic density along the aldehyde- and OsO_4-fixed nexus most frequently appears as a row of small diffuse densities lateral to each junctional membrane (Fig. 1*b*, *d*, and *f*) or as an amorphous electron-dense plaque along each junctional membrane. Each row of densities extends 25.6 SD 2.2 nm (n = 50) into the cytoplasm as measured from the central plane between the junctional membranes. The densities frequently appear to contact the junctional membranes by short stalks. The cytoplasmic density along the permanganate-fixed nexus normally appears as an amorphous plaque of variable density and extent (Fig. 2*a*, *c*, and *d*).

The presence and the morphology of the nexuses were not altered by slight variations in the aldehyde fixative, nor did they depend upon whether the fixative was perfused or applied to isolated bundles.

Other than its being frequently associated with the fascia adherens, the myocardial nexus does not appear to be preferentially localized along any specific region of the ventricular cell sarcolemma. This junction may be similar to the nexus (gap junction, author's term) reported by Baldwin (1) in frog atrium.

Width of the Frog Myocardial Nexus

Figure 5 illustrates the microdensitometric method used to reconstruct nexuses. The purpose of comparing myocardial and liver nexuses was to determine whether the two junctions were similar in width and structure (Figs. 1, 2, and 4*e*). The results of these measurements are presented in Table I.

The mean total widths of the aldehyde- and OsO_4-fixed nexuses and the permanganate-fixed nexuses in frog ventricle from microdensitometric measurements, 15.8 nm and 16.6 nm, respectively, are very similar to the width of liver nexuses, 16.6 nm. Direct measurements of the projected images gave an average width of 16.0 nm.

The width of the less electron-dense region (gap) between the junctional membranes of the aldehyde- and OsO_4-fixed myocardial nexus at the membrane apposition points is 1.8 nm, compared

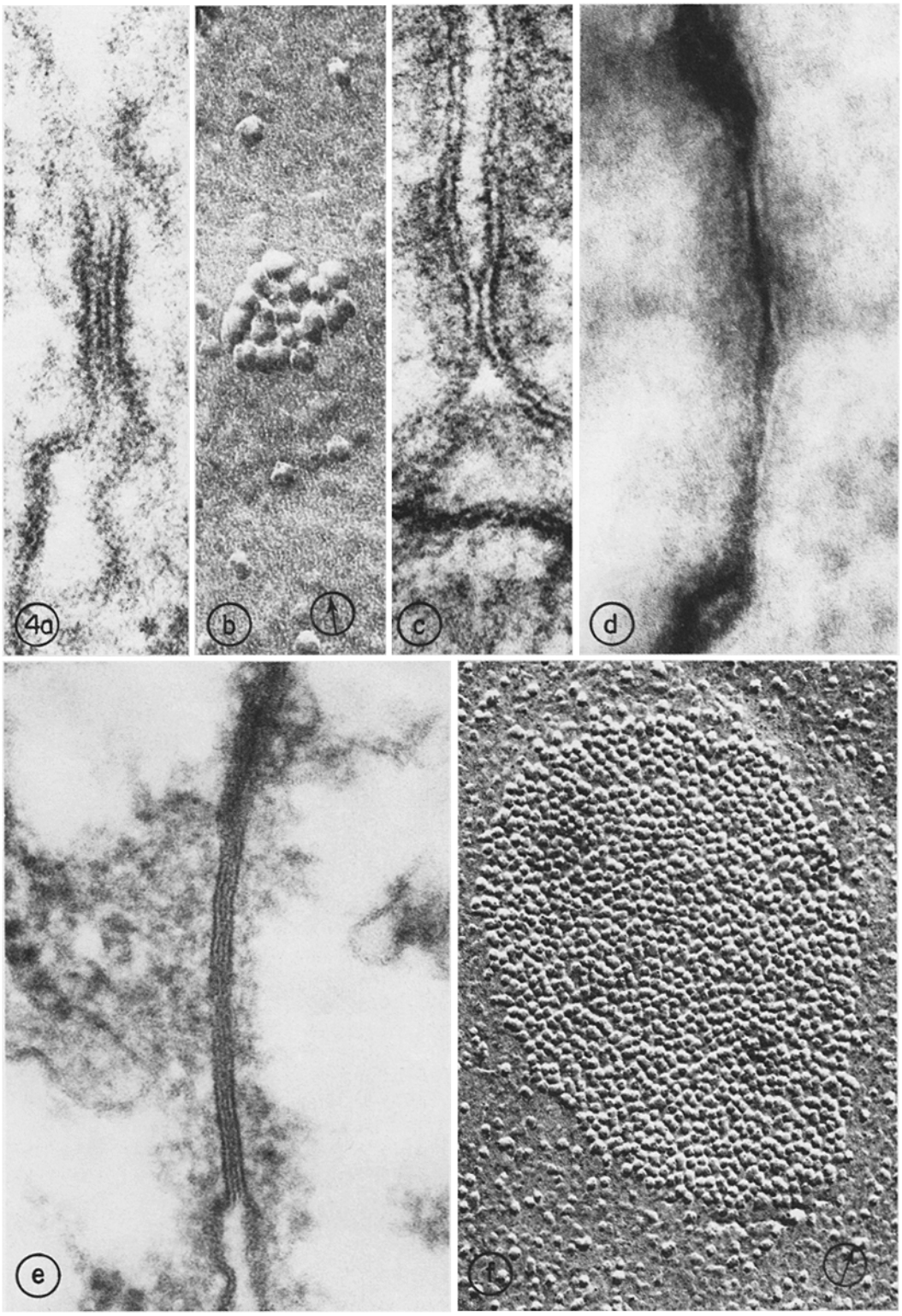

FIGURE 4 (*a*) A short septalaminar nexus in a thin section of an aldehyde- and OsO_4-fixed ventricle. × 340,000. (*b*) Freeze-fracture showing a small isolated cluster of particles on the PF face of the myocardial nexus. × 340,000. (*c*) A short pentalaminar nexus in a thin section of a permanganate-fixed ventricle. × 340,000. (*d*) Thin section of ruthenium red-filled myocardial nexus. × 340,000. (*e* and *f*) Appearance of liver nexus in thin section and on the PF face of freeze-fracture replica. Fig. 4*e*, × 190,000. Fig. 4*f*, × 150,000.

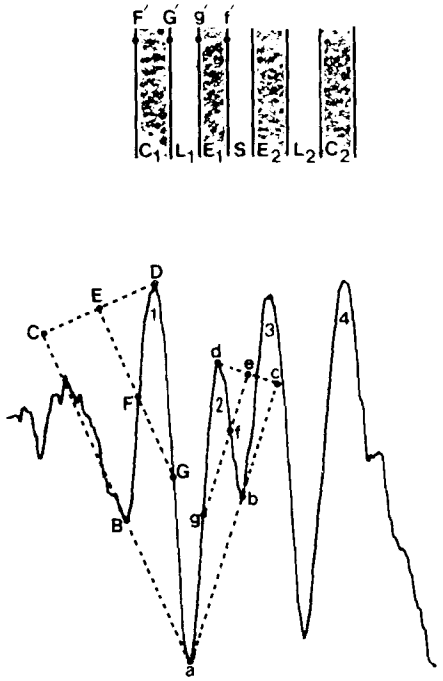

FIGURE 5 The method used to reconstruct the structure of the myocardial and liver nexuses is illustrated for the reconstruction of cytoplasmic lamella *1* (C_1) and extracellular lamella *1* (E_1). The construction for C_1 has four steps: (i) The baseline of peak 1 (line *aB*) was constructed from point (*a*), the base of the trough between peaks *1* and *2*, to point *B*, the point at which the curve of peak *1* first reveals roughness due to cytoplasmic densities along the membrane. (ii) Line *DC* was constructed through the apex of peak *1* (point *D*) perpendicular to the extension *BC* of line *aB*. (iii) The midpoint of line *DC* was determined. A line normal to *CD* at *E* establishes *F*, the half-peak height of peak *1*. (iv) The distance between lines *G'* and *F'* is the width of peak *1* at its half-peak height. The width of C_1 in the junction is determined by dividing the distance between lines *G'* and *F'* by the total specimen magnification. Cytoplasmic lamella *2* (C_2) is reconstructed and measured similarly. The method for reconstructing extracellular lamella *1* (E_1) is analogous to that for C_1, starting with the construction of the baseline peak *2* (line *ab*) from point (*a*), the base of the trough between peaks *1* and *2*, to point *b*. The remainder of the reconstruction steps for E_1 are identical to those for C_1. For convenience, the corresponding lines in the reconstruction of E_1 compared to that of C_1 are labeled with the same letters, but lower case. Extracellular lamella *2* (E_2) is reconstructed identically. The widths of the lipid bilayer lamallae (L_1, L_2) of each junctional membrane and the junctional intermembrane region (S) follow from the determination of the cytoplasmic and extracellular lamellae. The total widths of nonjunctional sarcolemma were determined from microdensitometric reconstructions in which the cytoplasmic and extracellular lamella were reconstructed by the procedure described for C_1.

to 2.0 nm for the liver nexus. These two junctions are further very similar with respect to the widths of their junctional membrane lamellae C_1, L_1, E_1, E_2, L_2, and C_2 (Table I).

Since the regions of membrane apposition in the permanganate-fixed myocardial nexus are pentalaminar, the junctional membrane lamellae of this nexus are not directly comparable to those of the aldehyde- and OsO_4-fixed heart or liver nexuses, but certain points are of interest. The mean width of the central electron-dense lamella of the pentalaminar membrane appositions, 3.9 nm, is less than the widths of the two extracellular lamellae plus "gap" (E_1 + Gap + E_2, Table I) of either the aldehyde- and OsO_4-fixed heart nexus or liver nexus. The cytoplasmic lamellae (C_1, C_2) and the electron-translucent bilayer lamellae (L_1, L_2) of the permanganate-fixed myocardial nexus are correspondingly wider (Table I), such that the total junctional width is similar to that of the aldehyde- and OsO_4-fixed nexuses.

Ruthenium Red

When ruthenium red was added to the post-aldehyde fixation buffer rinse and the OsO_4 fixative, it filled the entire extracellular space of the ventricular bundles with an amorphous, electron-dense precipitate. The precipitate was also present within the confines of the myocardial nexuses where it delineated the usual morphology of these junctions (Fig. 4*d*). The electron-dense precipitate filled the entire intrajunctional space of the nexus including the narrow 1.8-nm electron-translucent region between the junctional membranes at the regions of membrane apposition (Fig. 4*d*). This demonstates that the intrajunctional spaces, where the junctional membranes diverge and are 5–15 nm apart, are not sealed from the extracellular space (at least not postfixation).

Freeze-Cleavage

Freeze-cleavage of fixed and unfixed frog ventricle exposes extensive membrane fracture faces of the cardiac muscle cells. The fascia adherens, as expected from previous reports in other animals (26, 27), is not clearly identifiable on the membrane fracture faces. The nexus appears on the PF face as a very distinctive array of particles of

TABLE I

Microdensitometric Measurements of the Frog Myocardial and Liver Nexuses

	Frog cardiac nexus (aldehyde and OsO_4 Fixation) Mean ± SD (*n*)	Frog liver nexus (aldehyde and OsO_4 fixation) Mean ± SD (*n*)	Frog cardiac nexus (permanganate fixation) Mean ± SD (*n*)
	nm	*nm*	*nm*
Total junction width	15.8 ± 1.0 (25)	16.6 ± 0.9 (25)	16.6 ± 0.9 (11)
Cytoplasmic lamella 1 (C_1)	2.9 ± 0.4 (25)	3.2 ± 0.3 (25)	3.3 ± 0.4 (11)
Lipid bilayer lamella 1 (L_1)	2.3 ± 0.5 (25)	2.1 ± 0.2 (25)	2.8 ± 0.4 (11)
Extracellular lamella 1 (E_1)	2.2 ± 0.3 (19)	2.2 ± 0.3 (24)	
Junctional gap (S)	1.8 ± 0.2 (19)	2.0 ± 0.2 (24)	3.9 ± 0.8 (11)
Extracellular lamella 2 (E_2)	2.0 ± 0.2 (19)	2.1 ± 0.3 (24)	
Lipid bilayer lamella 2 (L_2)	2.4 ± 0.4 (25)	2.2 ± 0.3 (24)	2.9 ± 0.5 (11)
Cytoplasmic lamella 2 (C_2)	2.8 ± 0.4 (25)	3.0 ± 0.4 (25)	3.4 ± 0.5 (11)
Nonjunctional membrane width	7.8 ± 1.0 (11)		8.1 ± 0.5 (7)

uniform diameter arranged in up to nine linked or partial circles (Figs. 1*c*, *e*, 2*b*, and *e*). Frequently, small clusters of closely packed particles of a diameter similar to that of the particles in the circles are attached to the circles (Figs. 1 *c*, *e*, and 2 *c*), and rarely such clusters of closely packed particles appear alone on the fracture face (Fig. 4*b*).

The complete or nearly complete circles of particles are of uniform size with a mean circle diameter of 76.7 nm (Fig. 3*a*) and contain 20 particles. In general, only small nexuses consist entirely of closed circles of particles (Fig. 2*b*), while the larger nexuses consist of many linked partial circles, i.e. short arcs and C-shaped rows of particles (Figs. 1*c*, *e*, and 2*e*).

The surface enclosed by the circles or partial circles of particles appears very smooth and particle-free (Figs. 1*c*, *e*, 2*b*, and *e*), although occasionally one to two particles appear near the center of the circle (Fig. 2*e*). A particle-free zone usually surrounds the entire array of nexal particles (Figs. 1*c*, *e*, 2*b*, and *e*).

The majority of the nexal particles are very uniform in size and shape, but there is a small percentage of larger, more irregularly shaped particles (Fig. 2*b* and *e*) which may represent fusion of two or more particles. The distribution of particle diameters for the myocardial nexus is illustrated in Fig. 6 and is compared to the distribution of nexal particle diameters for the frog liver nexus. The mean diameter of the particles of the myocardial nexus is 10.4 nm compared to 10.3 nm (Fig. 6) for the liver nexus. If the larger irregular particles are included, the mean diameter of the particles in the myocardial nexus is 10.8 nm. The particles in the freeze-fractured myocardial nexus are thus very similar in diameter to the particles of the frog liver nexus.

The nexus appears on the EF-face as arrays of pits or grooves which are arranged in up to 9, or more, linked circles (Figs. 1*a*, 7*a*, *b*) often possessing small clusters of associated pits (Fig. 1*a*) corresponding to the small clusters of tightly packed particles attached to the circles on the PF face. The pits or grooves are unusually shallow and are best revealed in junctions shadowed at a very low angle with respect to the fracture face (Fig. 1*a*) such that the surface is seen in high relief. In such nexuses, the surface area enclosed by the circles of pits or grooves often appears to bulge out. The mean diameter of the circles of pits 77.3 nm (Fig. 3*c*) closely corresponds to the mean diameter of the circles of particles on the PF face.

Although the frog heart nexus does not normally cross-fracture to reveal both the nexal particles and pits or grooves on adjacent PF and EF faces, two examples of this type are shown in Fig. 7*a* and *b*. In Fig. 7*a*, several rings are present on the EF face, and at the transition from the EF face to the PF face the nexal particles are revealed. In Figure 7*b*, a single ring on the EF face is present and a small portion of the EF face has been fractured away to reveal the adjacent nexal particles on the PF face. In both of these examples, the particles appear to almost protrude to the surface of the EF face. Junctions of this type are rare because the transition of the cleavage plane from the PF face of one junctional membrane to the EF face of the other normally occurs at the border of the nexus of the frog heart, leaving the EF face abutting the side of the nexus (Fig. 7*c–e*).

Similar arrays of particles and pits or grooves arranged in circles were present in the freeze-cleave replicas of unfixed frog ventricle, thus demonstrating that the unusual arrangement of the nexal particles is not a result of fixation.

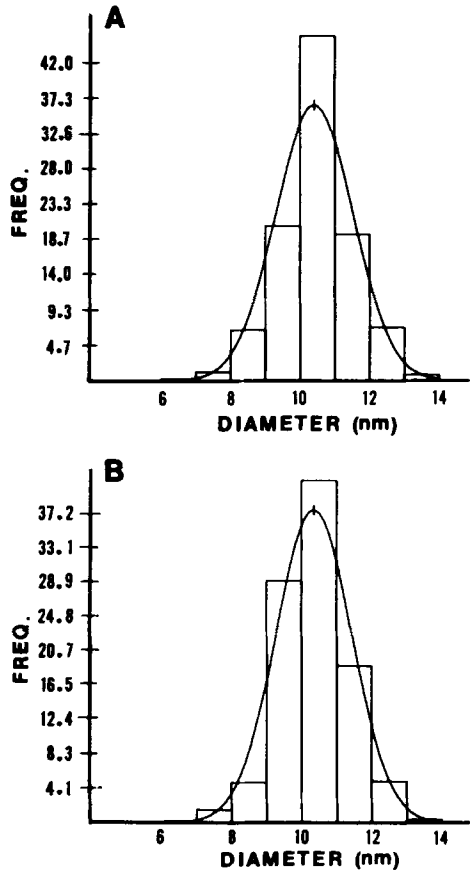

FIGURE 6 Histograms comparing the distributions of the diameters of particles of the freeze-fractured myocardial nexus (A) and liver nexus (B). The mean diameter of the myocardial nexal particle was 10.4 SD 1.1 nm (n = 537) and the mean diameter of the liver nexal particle was 10.3 SD 1.0 nm (n = 524).

DISCUSSION

Using thin-sectioning and freeze-cleavage techniques, we have demonstrated an unusual nexus in frog ventricle, a tissue previously reported to lack nexuses (38–40). The demonstration of this nexus provides a morphological basis for the spread of current electrotonically in this tissue (44) and is consistent with the widespread occurrence of nexuses in other vertebrate hearts (4, 20, 25, 26) and with the concept that nexuses are involved in the electrotonic coupling of cells (3–8, 13, 14, 16, 17, 28, 29).

Several lines of evidence described here support the view that this junction is a nexus. The width of the junction at the regions of membrane apposition in thin sections (Table I) is similar to the width of the frog liver nexus and corresponds well to the range of widths (15.0–18.0 nm) published for other nexuses (6, 10, 15, 18, 26). The width of the electron-lucent region (gap) between the junctional membranes of the uranyl acetate-*en bloc*-stained myocardial nexus at the points of closest membrane apposition is 1.8 nm, compared to 2.0 nm for the frog liver nexus, and again corresponds well to the published values for other nexuses (10, 18, 26, 35). In the freeze-fracture replicas, at regions where both the PF face of one junctional membrane and the EF face of the other are revealed at the particle or pit array the extracellular space is greatly reduced. In favorable cases, the cleavage plane through the junction clearly reveals the 10.4-nm diameter particles on the PF face of one junctional membrane contiguous with the pits or grooves on the EF face of the other (Fig. 7 *a* and *b*). This appearance is characteristic of freeze-fractured nexuses (11) and is consistent with current models of nexal structure (11, 26). Finally, although the diameter of the circularly arrayed particles (10.4 nm) is larger than the diameters (7–9 nm) usually reported for other freeze-fractured nexal particles (12, 26, 27, 34, 37), it corresponds well to the diameter of freeze-fractured particles of the frog liver nexus under our conditions.

The best evidence that the junctions in thin sections correspond to the nexus demonstrated by freeze-fracture is provided by the close similarity in the mean distance between the nexal-like membrane appositions along the length of the junction in thin sections and the diameter of the rings of particles and pits in the freeze-fractured nexus.

Model of the Frog Myocardial Nexus

Figure 8 presents a model for the frog ventricular nexus. In this model, the nexal subunits of each junctional membrane are arranged in arrays of linked circles. Each nexal subunit in one junctional membrane and the corresponding subunit in the other junctional membrane abut along the central plane between the junctional membranes. In common with other models of nexal structure (26), each nexal subunit is depicted as possessing a 1.0–2.0 nm diameter central channel, such that the abutment of corresponding nexal subunits in each junctional membrane forms a single channel from the cytoplasm of one cell to that of the other cell. McNutt and Weinstein (26, 27) and Staehelin (41) have reviewed the evidence for such intercellular transnexal channels. In the model, the junctional membranes are held in apposition in the

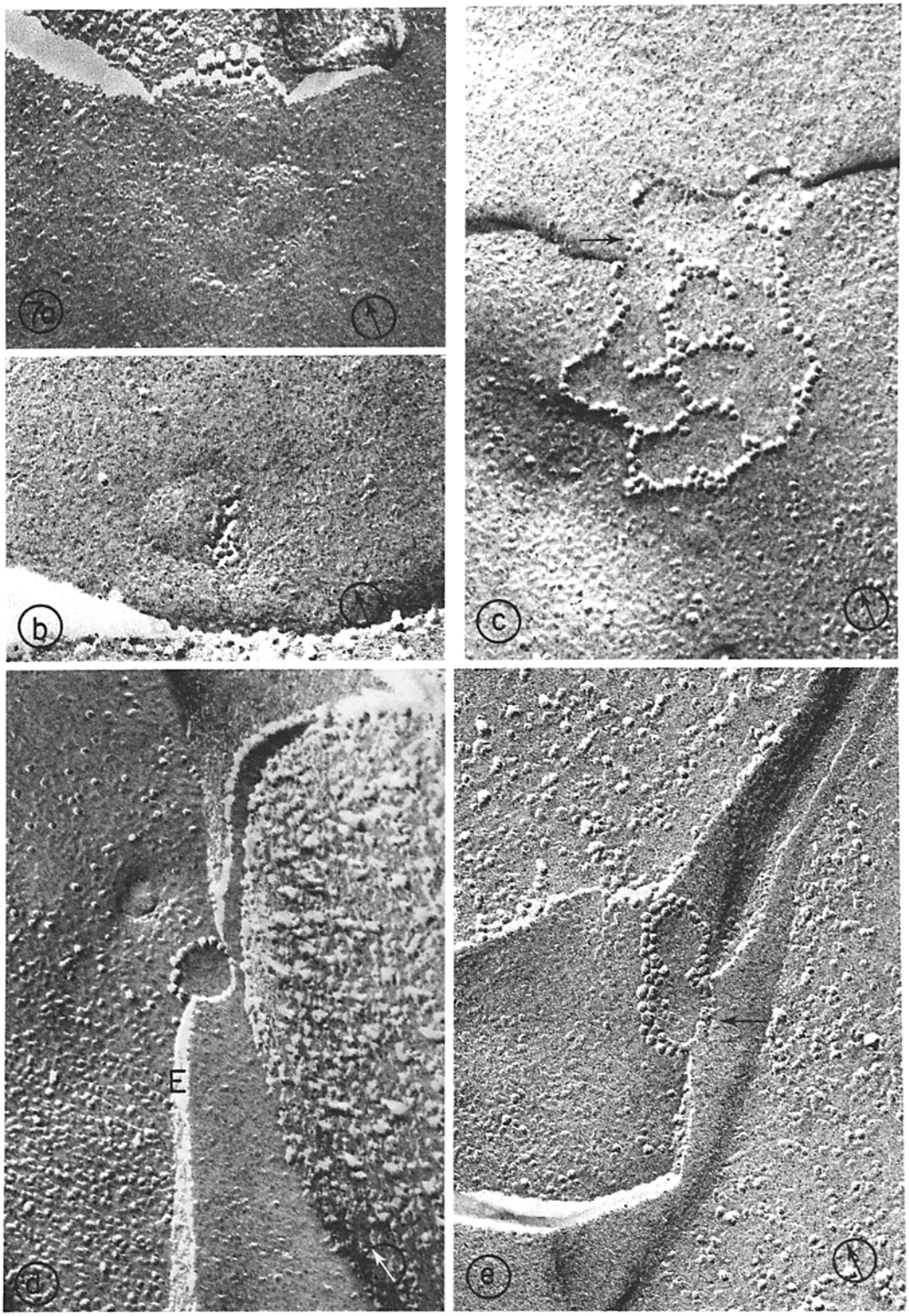

FIGURE 7 Freeze-cleavage showing myocardial nexuses at the transition of the cleavage plane from the PF face to the EF face. (*a* and *b*) Two predominantly EF face nexuses with adjacent 10.4-nm nexal particles on the PF face. Note that the particles appear to almost protrude to the surface of the EF face. × 160,000. (*c*, *d*, and *e*) Nexuses on the PF face illustrating the narrowing of the extracellular space (*E*) at the nexus. Note the perturbation of the EF face by the underlying nexal particles at the arrows in *c* and *e*. × 100,000.

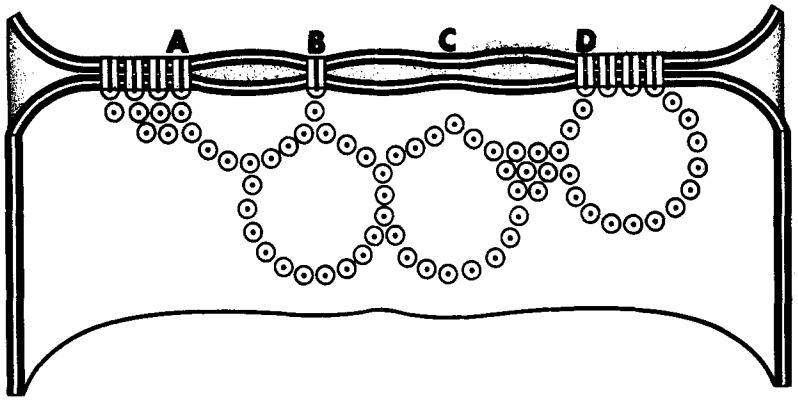

FIGURE 8 A model for the frog myocardial nexus. The small circles represent the nexal subunits bridging the junctional membranes. The black dot at the center of each circle represents a 1.0–2.0-nm pore through the nexal subunit. Points A, B, and D are membrane appositions of the junctional membranes. Point C is at an incomplete circle of nexal subunits.

regions where the nexal subunits abut but are free to bulge outwards in a domelike fashion from each other at the center of the circles of nexal subunits where nexal subunits are lacking.

If cut in cross section, the junction as indicated in the model would appear as a periodic series of membrane apposition points (points A, B, and D) separated by regions in which the membranes diverge. This appearance is similar to that of the myocardial nexuses in thin sections.

Since the freeze-cleavage replicas indicate that the circles of nexal particles are not always complete, an example of this is illustrated at point C in the model. If a transverse section through the model passes through one of these incomplete circles at the point where the circle is incomplete (point C), the junctional membranes will approach each other at this point because of the adjacent nexal subunits in the circle but will not come into apposition because there is no subunit at point C to hold them together. In the thin-sectioned nexus in Fig. 1*f*, the double arrow points to a region which is probably of this nature.

Additionally, the model illustrates that the slightly longer regions of membrane apposition present in some of the nexuses in thin sections may appear if the plane of the transverse section through the junction lies tangential to one of the circles of nexal subunits (point D), or if it passes through a cluster of tightly packed nexal subunits attached adjacent to the circles (point A). The model explains the difference between the frog myocardial nexus and most other vertebrate nexuses seen in thin sections.

At present, it is unclear why the frog myocardial nexus has this unusual structure compared to other nexuses. Decker and Friend (12) have suggested that nexuses consisting of strands of particles may represent stages in the development of vertebrate nexuses. This is unlikely in the frog ventricle, since the unusual nexuses are the predominant form present in the adult heart. The recent demonstration of unusual nexuses between the lacis and mesangial cells of the kidney (33), between vertebrate photoreceptor cells (34), in crayfish ganglia (30, 31, 32), in the ciliary epithelium of the albino eye (22), and in mammalian arteries and veins (37) makes it probable that nexuses with unusual morphology may be more common than previously recognized.

Addendum

Since submission of this manuscript, results similar to those described here have been reported for frog atrial fibers (F. Mazet and J. Cartaud, 1976. Freeze fracture studies of frog atrial fibres. *J. Cell. Sci.* **22**:427–434).

We wish to thank David E. Colflesh for his superb technical assistance and Vivian Schotter for her generous help in preparing the manuscript. In addition we would like to especially thank Dr. N. B. Gilula for his invaluable assistance in teaching us the freeze-fracture technique and in advising us on interpretation of the images.

The investigation was supported by a grant from the National Institutes of Health GM 20628. Dr. Brink was a recipient of National Institutes of Health postdoctoral fellowship GM 05231.

Portions of this work were reported in the Abstracts of the 30th Annual Meeting of The Society of General Physiologists 1976.

Received for publication 17 November 1976, and in revised form 21 January 1977.

REFERENCES

1. BALDWIN, K. 1970. The fine structure and electrophysiology of heart muscle cell injury. *J. Cell Biol.* **46**:455-476.
2. BARR, L., and W. BERGER. 1964. The role of current flow in the propagation of cardiac muscle action potentials. *Pfluegers Arch. Gesamte. Physiol. Menschen Tiere.* **279**:192-194.
3. BARR, L., W. BERGER, and M. M. DEWEY. 1968. Electrical transmission at the nexus between smooth muscle cells. *J. Gen. Physiol.* **51**:347-368.
4. BARR, L., M. M. DEWEY, and W. BERGER. 1965. Propagation of action potentials and the structure of the nexus in cardiac muscle. *J. Gen. Physiol.* **48**:797-823.
5. BENNETT, M. V. L., Y. NAKAJIMA, and G. PAPPAS. 1967. Physiology and ultrastructure of electrotonic junctions. I. Supramedullary neurons. *J. Neurophysiol.* **30**:161-179.
6. BENNETT, M. V. L., Y. NAKAJIMA, and G. PAPPAS. 1967. Physiology and ultrastructure of electrotonic junctions. III. Giant electromotor neurons of *Malapterurus electricus*. *J. Neurophysiol.* **30**:209-235.
7. BENNETT, M. V. L., G. PAPPAS, E. ALJURE, and Y. NAKAJIMA. 1967. Physiology and ultrastructure of electrotonic junctions. II. Spinal and medullary electromotor nuclei in moryrid fish. *J. Neurophysiol.* **30**:180-208.
8. BENNETT, M. V. L., G. PAPPAS, M. GIMENEZ, and Y. NAKAJIMA. 1967. Physiology and ultrastructure of electrotonic junctions. IV. Medullary electromotor nuclei in gymnotid fish. *J. Neurophysiol.* **30**:236-300.
9. BRANTON, D., S. BULLIVANT, N. B. GILULA, M. J. KARNOVSKY, H. MOORE, K. MÜHLETHALER, D. H. NORTHCOTE, L. PACKER, B. SATIR, P. SATIR, V. SPETH, L. A. STAEHELIN, R. L. STEERE, and R. S. WEINSTEIN. 1975. Freeze-etching nomenclature. *Science (Wash. D. C.)* **190**:54-56.
10. BRIGHTMAN, M., and T. REESE. 1969. Junctions between intimately apposed cell membranes in the vertebrate brain. *J. Cell Biol.* **40**:648-677.
11. CHALCROFT, J., and S. BULLIVANT. 1970. An interpretation of liver cell membrane and junction structure based on observation of freeze-fracture replicas of both sides of the fracture. *J. Cell Biol.* **47**:49-60.
12. DECKER, R., and D. S. FRIEND. 1974. Assembly of gap junctions during amphibian neurulation. *J. Cell Biol.* **62**:32-48.
13. DEWEY, M. M., and L. BARR. 1962. Intercellular connections between smooth muscle cells: the nexus. *Science (Wash. D. C.)*. **137**:670-672.
14. DEWEY, M. M., and L. BARR. 1964. A study of the structure and distribution of the nexus. *J. Cell Biol.* **23**:553-585.
15. DEWEY, M. M., and L. BARR. 1970. Some considerations about the structure of cellular membranes. Current Topics in Membranes and Transport. F. Bronner and A. Kleinzeller, editors. Academic Press, Inc., **1**:1.
16. DREIFUSS, J., L. GIRARDIER, and W. FORSSMANN. 1966. Etude de la propagation de l'excitation dans la ventricule de rat at moyen de solutions hypertoniques. *Pfluegers Arch Gesamte. Physiol. Menschen Tiere.* **282**:13-33.
17. GILULA, N. B., D. REEVES, and A. STEINBACH. 1972. Metabolic coupling, ionic coupling and cell contacts. *Nature (Lond.)*. **235**:262-265.
18. GOODENOUGH, D., and J. REVEL. 1970. A fine structural analysis of intercellular junctions in the mouse liver. *J. Cell Biol.* **45**:272-290.
19. GOSHIMA, K. 1970. Formation of nexuses and electrotonic transmission between myocardial and FL cells in monolayer culture. *Exp. Cell Res.* **63**:124-130.
20. HIRAKOW, R. 1970. Ultrastructural characteristics of the mammalian and Sauropsidian heart. *Am. J. Cardiol.* **25**:195-203.
21. KARNOVSKY, M. J. 1965. A formaldehyde-glutaraldehyde fixative of high osmolarity for use in electron microscopy. *J. Cell Biol.* **27**(2, Pt. 2):137-138*a*. (Abstr.).
22. KOGON, M., and G. PAPPAS. 1975. Atypical gap junctions in the ciliary epithelium of the albino rabbit eye. *J. Cell Biol.* **66**:671-675.
23. LUFT, J. 1971. Ruthenium red and violet. I. Chemistry, purification and methods of use for electron microscopy and mechanism of action. *Anat. Rec.* **171**:347-368.
24. LUFT, J. 1971. Ruthenium red and Violet. II. Fine structural localization in animal tissue. *Anat. Rec.* **171**:369-415.
25. MARTINEZ-PALOMO, A., and R. MENDEZ. 1971. Presence of gap junctions between cardiac cells in the heart of non-mammalian species. *J. Ultrastruct. Res.* **37**:592-600.
26. MCNUTT, N., and R. WEINSTEIN. 1970. The ultrastructure of the nexus. A correlated thin-section and freeze-cleave study. *J. Cell Biol.* **47**:666-688.
27. MCNUTT, N., and R. WEINSTEIN. 1973. Membrane ultrastructure of mammalian intercellular junctions. *Progress Biophys. Mol. Biol.* **26**:45-101.
28. PAPPAS, G., Y. ASADA, and M. BENNETT. 1971. Morphological correlates of increased coupling resistance of electrotonic synapse. *J. Cell Biol.* **49**:173-188.
29. PAYTON, B., M. BENNETT, and G. PAPPAS. 1969. Permeability and structure of junctional membranes at an electrotonic synapse. *Science (Wash. D. C.)*. **166**:1641-1643.
30. PERACCHIA, C. 1973. Low resistance junctions in Crayfish. I. Two arrays of globules in junctional membranes. *J. Cell Biol.* **57**:54-65.
31. PERACCHIA, C. 1973. Low resistance junctions in

crayfish. II. Structural details and further evidence for intercellular channels by freeze-fracture and negative staining. *J. Cell Biol.* **57**:66–76.

32. PERACCHIA, C., and A. DULHUNTY. 1976. Low resistance junctions in crayfish. Structural changes with functional uncoupling. *J. Cell Biol.* **70**:419–439.
33. PRICAM, C., F. HUMBERT, A. PERRELET, and L. ORCI. 1974. Gap junctions in mesangial and lacis cells. *J. Cell Biol.* **63**:349–354.
34. RAVIOLI, E., and N. B. GILULA. 1975. Intramembrane organization of specialized contacts in the outer plexiform layer of the retina. A freeze-fracture study in monkeys and rabbits. *J. Cell Biol.* **65**:192.
35. REVEL, J., and M. J. KARNOVSKY. 1967. Hexagonal arrays of subunits in intercellular junctions of the mouse heart and liver. *J. Cell Biol.* **33**:C7–C12.
36. REYNOLDS, E. 1963. The use of lead citrate at high pH as an electron-opaque stain in electron microscopy. *J. Cell Biol.* **17**:208–212.
37. SIMIONESCU, M., N. SIMIONESCU, and G. E. PALADE. 1976. Segmental differentiations of cell junctions in the vascular endothelium. Arteries and veins. *J. Cell Biol.* **68**:705–723.
38. SOMMER, J., and E. JOHNSON. 1969. Cardiac muscle, a comparative ultrastructural study with special reference to frog and chicken hearts. *Z. Zellforsch. Mikrosk. Anat.* **98**:437–468.
39. SOMMER, J., and E. JOHNSON. 1970. Comparative ultrastructure of cardiac cell membrane specializations. A review. *Am. J. Cardiol.* **25**:184–194.
40. SOMMER, J., and R. WAUGH. 1976. The ultrastructure of the mammalian cardiac muscle cell—with special emphasis on the tubular membrane system. *Am. J. Pathol.* **82**:192–217.
41. STAEHELIN, L. 1974. Structure and function of intercellular junctions. *Int. Rev. Cytol.* **39**:191–283.
42. STALEY, N., and E. BENSON. 1968. The ultrastructure of frog ventricular cardiac muscle and its relationship to mechanisms of excitation—contraction coupling. *J. Cell Biol.* **38**:99–114.
43. TRAUTWEIN, W., S. KUFFLER, and C. EDWARDS. 1956. Changes in membrane characteristics of heart muscle during inhibition. *J. Gen. Physiol.* **40**:135–145.
44. VAN DER KLOOT, W., and B. DANE. 1964. Conduction of the action potential in the frog ventricle. *Science* (*Wash. D. C.*). **146**:74–75.
45. WEIDMANN, S. 1952. The electrical constants of Purkinje fibres. *J. Physiol.* (*Lond.*). **118**:348–360.
46. WEIDMANN, S. 1970. Electrical constants of trabecular muscle from mammalian heart. *J. Physiol.* (*Lond.*). **210**:1041–1054.
47. WOODBURY, J., and W. CRILL. 1961. On the problem of impulse conduction in the atrium. *In* Nervous Inhibition. E. Florey, editor. Pergamon Press Ltd., Oxford. 124–125.